Fidelity, fidelity susceptibility, and von Neumann entropy to characterize the phase diagram of an extended Harper model

Longyan Gong[1,2,3,*] and Peiqing Tong[2,†]
[1]*Department of Mathematics, Nanjing Normal University, Nanjing 210097, China*
[2]*Department of Physics, Nanjing Normal University, Nanjing 210097, China*
[3]*Department of Mathematics and Physics, Center of Microfluidics Optics and Technology, Nanjing University of Posts and Telecommunications, Nanjing 210003, China*
(Received 11 July 2008; revised manuscript received 22 August 2008; published 17 September 2008)

In an extended Harper model, the fidelity for the two lowest band-edge states corresponding to different model parameters, the fidelity susceptibility and the von Neumann entropy of the lowest band-edge states, and the spectrum-averaged von Neumann entropy are studied numerically. The fidelity is near one when parameters are in the same phase or same phase boundary; otherwise it is close to zero. There are drastic changes in fidelity when one parameter is at phase boundary. For the fidelity susceptibility the finite scaling analysis is performed. The critical exponents α, β, and ν depend on system sizes for the metal-metal phase transition, while this is not so for the metal-insulator phase transition. At both phase transitions $\nu/\alpha \approx 2$. The von Neumann entropy is near one for the metallic phase, while it is small for the insulating phase. There are sharp changes in the von Neumann entropy at phase boundaries. According to the variations of the fidelity, fidelity susceptibility, and the von Neumann entropy with model parameters, the phase diagram, which includes two metallic phases and one insulating phase separated by three critical lines with one bicritical point, can be completely characterized. These numerical results indicate that the three quantities are suited for revealing all the critical phenomena in the model.

DOI: 10.1103/PhysRevB.78.115114 PACS number(s): 71.30.+h, 03.67.−a, 71.23.Ft

I. INTRODUCTION

In recent years, tools from the quantum-information theory,[1,2] specifically the ground-state fidelity[3] and quantum entanglement,[4,5] have been widely exploited to characterize quantum phase transitions (QPTs).[6] For example, in one-dimensional *XY* and Dicke models, the fidelity between two ground states corresponding to slightly different values of the parameters drastically decreases at phase-transition points.[3] Subsequently, similar properties are also found in fermionic,[7,8] bosonic systems,[9,10] and other various spin systems.[11,12] Very recently, fidelity susceptibility (FS) (the second derivative of fidelity) is introduced to signal QPTs in one-dimensional Hubbard models,[13–15] the Lipkin-Meshkov-Glick model,[16] the Kitaev honeycomb model,[17] and various spin systems.[18–20] It is found that FS is more crucial than fidelity itself for it does not depend on the slightly different values of model parameters. In Refs. 21 and 22, the fidelity between arbitrary two ground states is studied in one-dimensional quantum Ising model. Singularities are found in fidelity surfaces for QPTs.[22] The main advantage of the fidelity in identifying QPTs is that[18] it does not need *a priori* knowledge of the order parameter, topology, etc., since the fidelity is a purely Hilbert-space geometrical quantity.

At the same time, quantum entanglement has been extensively applied in condensed-matter physics.[23–29] For example, quantum entanglement measured by the von Neumann entropy has been studied in the Hubbard model for the dimer case,[23] in the extended Hubbard model for different band fillings,[24] in quantum small-world networks,[25] and in low-dimensional semiconductor systems.[26] It is found that the von Neumann entropy is suitable for analyzing the interplay between itinerant and localized features,[23] as well as characterizing quantum phase transition[24,27] and the localization-delocalization transition of electron states.[25,28,29]

On the other hand, since the Hofstadter butterfly energy spectrum was found in 1976,[30] the problem of electrons in two-dimensional periodic potential in a magnetic field has attracted much attention.[31–36] After fixing the quasimomentum in one of the directions, a one-dimensional quasiperiodic system called the Harper model is deduced.[30] The system shows interesting metal-insulator transitions (MITs).[32,33] Considering the next-nearest-neighbor hopping electrons on the square lattice in a uniform magnetic field, an extended Harper model is proposed[34] and studied extensively.[35] Very recently, a similar extended Harper model is introduced from two-dimensional electrons on the triangular lattice in a uniform magnetic field and its phase diagram has a very rich structure.[36]

Considering the above two aspects, we perform detailed studies of the fidelity between arbitrary two quantum states, FS and von Neumann entropy for the extended Harper model.[36] For each of the three quantities, there are drastic changes at phase boundaries; i.e., the phase diagram can be distinguished according to the variations of the quantities with model parameters. Our studies prove that the two tools, fidelity and von Neumann entropy, borrowed from the quantum-information theory, are well enough to identify phase transitions in the system.

The paper is organized as follows: In Sec. II the extended Harper model and the definitions of fidelity, FS, and von Neumann entropy are introduced. In Sec. III the numerical results are presented. We present our conclusions and discussions in Sec. IV.

II. EXTENDED HARPER MODEL, FIDELITY, FIDELITY SUSCEPTIBILITY, AND VON NEUMANN ENTROPY

A. Extended Harper model

The tight-binding Hamiltonian for an electron moving on a triangular lattice in a magnetic field[36] can be reduced to

$$H = -\sum_n [t_a + t_c e^{-2\pi i\phi(n-1/2)+ik_y}]c_n^\dagger c_{n-1} - \sum_n [t_a + t_c e^{2\pi i\phi(n+1/2)-ik_y}]c_n^\dagger c_{n+1} - 2\sum_n t_b \cos(2\pi\phi n + k_y)c_n^\dagger c_n, \quad (1)$$

where t_a, t_b, and t_c are the hopping integrals for each bond on the triangular lattice, $\phi/2$ is a uniform magnetic flux within each triangle, k_y is a momentum in the y direction, and $c_n^\dagger$ (c_n) is the creation (annihilation) operator of the nth site in the x direction.

Letting $|n\rangle$ denote $|0,\ldots,1_n,\ldots,0\rangle$, the general eigenstate of an electron with eigenenergy E_γ is

$$|\Psi_\gamma\rangle = \sum_n \psi_n^\gamma |n\rangle = \sum_n \psi_n^\gamma c_n^\dagger |0\rangle, \quad (2)$$

where ψ_n^γ is the amplitude of the γth eigenstate at the nth site. If we set $\lambda = 2\frac{t_b}{t_a}$ and $\mu = \frac{t_c}{t_a}$ and t_a is taken as units, eigenvalue equation (1) (Ref. 36) becomes

$$-[1+\mu e^{-2\pi i\phi(n-1/2)+ik_y}]\psi_{n-1} - [1+\mu e^{2\pi i\phi(n+1/2)-ik_y}]\psi_{n+1} - \lambda\cos(2\pi\phi n + k_y)\psi_n = E\psi_n. \quad (3)$$

The model was studied by Ino and Kohmoto.[36] The corresponding phase diagram is shown in Fig. 1. In regions I and III the wave functions (spectra) are extended (absolutely continuous), and in region II the wave functions are localized (pure points). On the three boundary lines, the wave functions (spectra) are critical (singular continuous). Besides the traditional MIT, there are transitions between the two metallic phases; i.e., metal-metal transitions (MMTs). At the bicritical point where the triangular lattice symmetry is retained, both level statistics and multifractal analysis show quantitatively different behaviors from those of other critical points.

At $\mu=0$ and when ϕ is irrational, Eq. (3) is reduced to the Harper equation. Intensively analytical and numerical studies[32,33] for the Harper model show that for $\lambda>2$ the spectrum is pure-point-like and all eigenstates are exponentially localized. For $\lambda<2$ the spectrum becomes continuous with delocalized eigenstates corresponding to ballistic classical motion. For $\lambda=2$ the situation is critical with a singular-continuous multifractal spectrum and eigenstates. MIT can occur at $\lambda=2$.

B. Fidelity

We directly diagonalize eigenvalue equation (3) at different values (λ,μ) and get all the eigenvalues E_γ and the corresponding eigenstates $|\Psi_\gamma\rangle$. Traditionally, the ground-state fidelity (fidelity susceptibility) in spin and many-electron systems are studied.[1,3,21,22] Similarly for single-particle systems, we define fidelity as

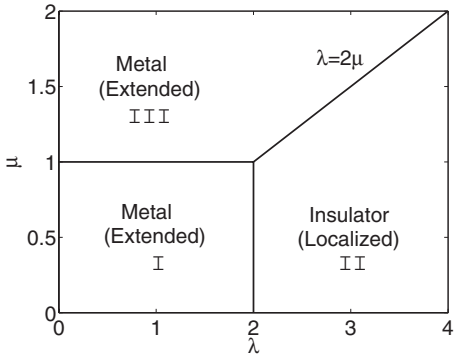

FIG. 1. Phase diagram of the extended Harper model.

$$F(\lambda,\mu;\lambda_0,\mu_0) = |\langle\Psi_0(\lambda,\mu)|\Psi_0(\lambda_0,\mu_0)\rangle|, \quad (4)$$

where $\Psi_0(\lambda_0,\mu_0)$ is the eigenstate of the lowest-energy eigenvalue for the system with parameters (λ_0,μ_0). Obviously, $F=1$ if $\lambda=\lambda_0$ and $\mu=\mu_0$.

C. Fidelity susceptibility

Similarly as shown in Ref. 3, the fidelity for the two lowest edge states with slightly different parameter values is defined as

$$F(q) = |\langle\Psi_0(q)|\Psi_0(q+\delta q)\rangle|. \quad (5)$$

For simplicity, a certain path $q=q(\lambda,\mu)$ in parameter spaces can always be supposed. Then the FS can be calculated as[13,17,37]

$$\chi_F = \lim_{\delta q\to 0}\frac{-2\ln F(q)}{\delta q^2} = \sum_{a=\lambda,\mu;b=\lambda,\mu} g_{a,b}n^a n^b, \quad (6)$$

where $n^\lambda = \partial q/\partial\lambda$ ($n^\mu = \partial q/\partial\mu$) denotes the tangent unit vector at a parameter point (λ,μ). For the present model, let us define the driving Hamiltonians as

$$H_\lambda = -\sum_n \cos(2\pi\phi n + k_y)c_n^\dagger c_n \quad (7)$$

and

$$H_\mu = -\sum_n [e^{-2\pi i\phi(n-1/2)+ik_y}]c_n^\dagger c_{n-1} - \sum_n [e^{2\pi i\phi(n+1/2)-ik_y}]c_n^\dagger c_{n+1}. \quad (8)$$

We have

$$g_{ab} = \sum_{\gamma\neq 0}\frac{\langle\Psi_\gamma(q)|H_a|\Psi_0(q)\rangle\langle\Psi_0(q)|H_b|\Psi_\gamma(q)\rangle}{(E_\gamma - E_0)^2}. \quad (9)$$

D. von Neumann entropy

The general definition of entanglement is based on the von Neumann entropy.[38] For an electron in the system, there are two local states at each site, i.e., $|0\rangle_n$ and $|1\rangle_n$. The local density matrix ρ_n is defined[23–25,29] as

$$\rho_n = z_n|1\rangle_{nn}\langle 1| + (1-z_n)|0\rangle_{nn}\langle 0|, \tag{10}$$

where $z_n = \langle\Psi_\gamma|c_n^\dagger c_n|\Psi_\gamma\rangle = |\psi_n^\gamma|^2$ is the local occupation number at the nth site. Consequently, the corresponding von Neumann entropy related to the nth site is

$$E_{vn}^\gamma = -z_n \log_2 z_n - (1-z_n)\log_2(1-z_n). \tag{11}$$

For nonuniform systems, the value of E_{vn}^γ depends on the site position n. At an eigenstate $|\Psi_\gamma\rangle$, we define the site-averaged von Neumann entropy as

$$E_v^\gamma = \frac{1}{N}\sum_{n=1}^{N} E_{vn}^\gamma, \tag{12}$$

where N is the system size. Definition (12) shows that for an extended state $\psi_n^\gamma = \frac{1}{\sqrt{N}}$ for all n and $E_v^\gamma = -\frac{1}{N}\log_2\frac{1}{N} - (1-\frac{1}{N})\log_2(1-\frac{1}{N}) \approx \frac{1}{N}\log_2 N$ at $N\to\infty$, and that for a localized state $\psi_n^\gamma = \delta_{nn^\circ}$ (n° is a given site) and $E_v^\gamma = 0$. In the paper all the values of E_v^γ and E_{vn}^γ are scaled by $\frac{1}{N}\log_2 N$. From the two examples, we know the scaled E_v^γ is near one when eigenstates are extended and near zero when eigenstates are localized. Henceforth, we omit "scaled" for simplicity.

In order to analyze the influence of system parameters on the von Neumann entropy for all the eigenstates, we define a spectrum-averaged von Neumann entropy as a further gross measure, i.e.,

$$\langle E_v\rangle = \frac{1}{M}\sum_{\gamma} E_v^\gamma, \tag{13}$$

where M is the number of all the eigenstates.

III. NUMERICAL RESULTS

In numerical calculations, without loss of generality, we set $k_y = 0$. As a typical case, $\phi = (\sqrt{5}-1)/2$. In fact as customary in the context of quasiperiodic system, the value of ϕ may be approximated by the ratio of successive Fibonacci numbers: $F_m = F_{m-2} + F_{m-1}$, with $F_0 = F_1 = 1$. In this way, choosing $\phi = F_{m-1}/F_m$ and system size $N = F_m$, we can obtain the periodic approximant for the quasiperiodic potential. We directly diagonalize eigenvalue equation (3) and get all the eigenvalues and the corresponding eigenstates. From formulas (4)–(13), we can obtain the fidelity $F(\lambda,\mu;\lambda_0,\mu_0)$, the FS χ_F, the site-averaged von Neumann entropy E_v^γ, and the spectrum-averaged von Neumann entropy $\langle E_v\rangle$. Henceforth, for simplicity we denote F as $F(\lambda,\mu;\lambda_0,\mu_0)$. In all the figures the system size N is chosen to be the Fibonacci number 987 unless specially stated.

A. Fidelity

In metallic phase I, metallic phase III, and insulating phase II, we choose $(\lambda_0,\mu_0) = (1.0,0.5)$, $(2.0,1.5)$, and $(3.0,0.75)$ as examples, respectively. The corresponding fidelity F varying with parameters λ and μ are shown in Fig. 2. At the same time, the contour maps of the fidelity are also shown. It shows that when parameters are at the same phase, the fidelity is near one; otherwise, the fidelity is very small. It is interesting that, though phases I and III are both metallic

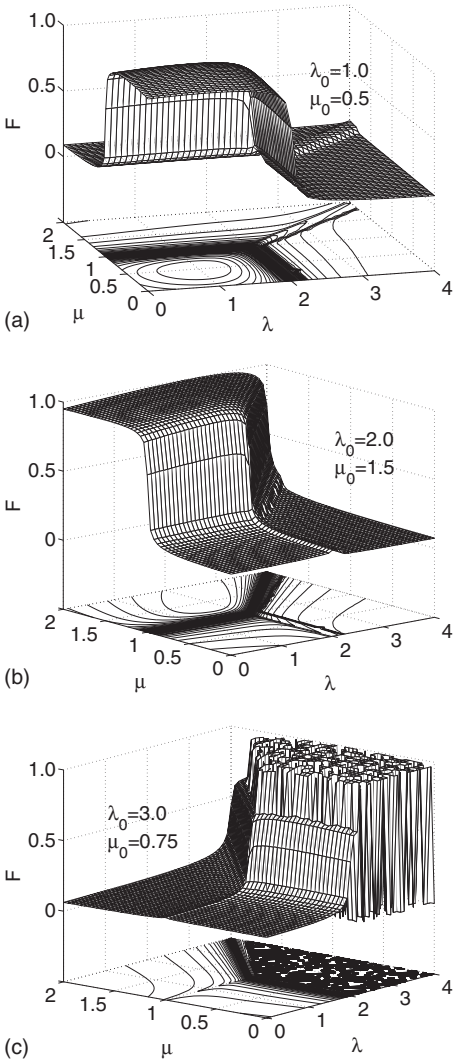

FIG. 2. The fidelity $F(\lambda,\mu;\lambda_0,\mu_0)$ and its contour map as functions of (λ,μ) at (a), (b), and (c) for $(\lambda_0,\mu_0) = (1.0,0.5)$, $(2.0,1.5)$, and $(3.0,0.75)$, which correspond to the system in metal phase I, metal phase III, and insulator phase II, respectively.

phases and the corresponding wave functions are all extended, the fidelity is small when parameters are in the two phases. This can be understood from the corresponding "classical orbit" Hamiltonian:[36] For phase I, the contour lines of the Hamiltonian are extended in the x direction but localized in the y direction, while for phase III, the contour lines are extended in the $x+y$ direction but localized in the $x-y$ direction. Therefore, the two phases are different. At the same time, these contour maps of fidelity divide the parameter space into different regions, in good agreement with the phase diagram shown in Fig. 1. Compared with the fidelities shown in Figs. 2(a) and 2(b), the fidelity in Fig. 2(c) changes more drastically with model parameters. It is because the band-edge states in insulating phase II may be localized in different space regions and the overlaps of these states may be large or small.

At the three phase boundaries, we choose $(\lambda_0,\mu_0) = (1.0,1.0)$, $(2.0,0.5)$, and $(3.0,1.5)$ as examples, which correspond to the system at the boundaries between phases I and

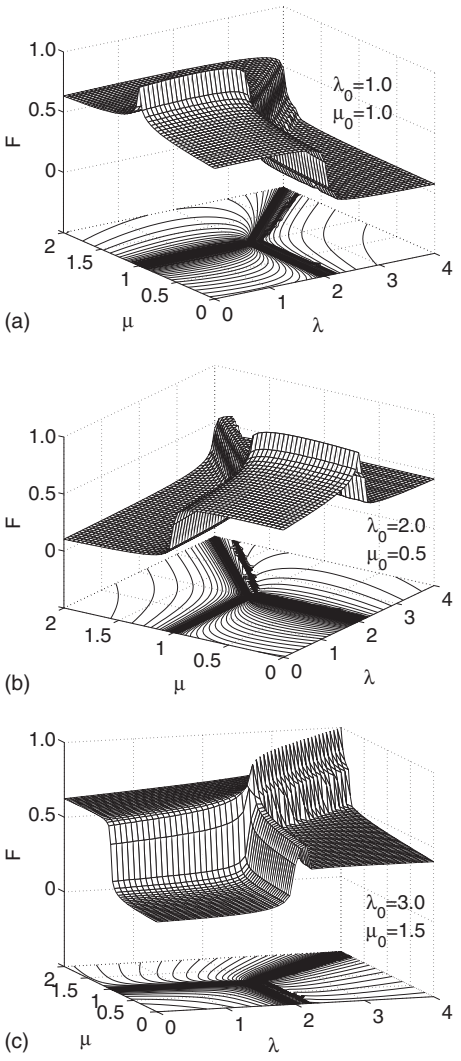

FIG. 3. The fidelity $F(\lambda,\mu;\lambda_0,\mu_0)$ and its contour map as functions of (λ,μ) at (a), (b), and (c) for $(\lambda_0,\mu_0)=(1.0,1.0)$, (2.0,0.5), and (3.0,1.5), which correspond to the system at the phase boundaries between I and III, I and II, and III and II, respectively.

III, phases I and II, and phases III and II, respectively. The fidelity F varying with λ and μ are shown in Fig. 3. It shows that when the parameters (λ,μ) and (λ_0,μ_0) are at the same critical line, the fidelity is near one; otherwise, the fidelity is relatively small. It is interesting that if a point (λ_0,μ_0) in the critical line between phases I and II (phases I and II; phases II and III), the fidelity in both phases is relatively large. Similarly as shown in Fig. 2, these contour maps of fidelity also divide the parameter space into three regions, which are the same as the phase diagram shown in Fig. 1.

At the bicritical point $(\lambda_0,\mu_0)=(2.0,1.0)$, the fidelity F and its contour map as functions of λ and μ are plotted in Fig. 4. It shows that when $(\lambda,\mu)=(2.0,1.0)$, F is maximal and equal to one; when (λ,μ) at the three critical lines, F becomes relatively small; and when (λ,μ) in phases I–III, F becomes relatively smaller. All these certify that the bicritical point itself is different from other points, in agreement with the conclusion that the bicritical point is a particular critical point as investigated in Ref. 36. At the same time, the contour of fidelity can reflect the phase diagram shown in Fig. 1.

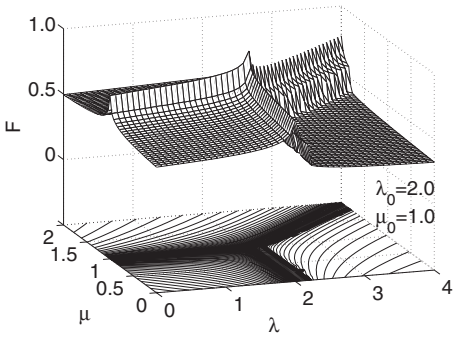

FIG. 4. The fidelity $F(\lambda,\mu;\lambda_0,\mu_0)$ and its contour map as functions of (λ,μ) for $(\lambda_0,\mu_0)=(2.0,1.0)$, which corresponds to the system at the bicritical point.

B. Fidelity susceptibility

According to the definition of FS in Eq. (6), its values depend on g_{ab} and a specific direction of parameter path $q=q(\lambda,\mu)$.[17] The tangent unit vector (n^λ,n^μ) which defines the direction may be different, though g_{ab} does not depend on parameter paths. In the following, the FS for $(n^\lambda,n^\mu)=(0,1)$, $(1,0)$, and $(1/\sqrt{5},-2/\sqrt{5})$ are shown in Figs. 5(a)–5(c), respectively, which correspond to that only μ changes, only λ changes, and both of them change simultaneously.

Figure 5 shows the $\chi_F(\lambda,\mu)$ for three different parameter paths. In Fig. 5(a), only the driving Hamiltonian H_μ affects the values of χ_F. From the corresponding contour map, the boundaries between metallic phase III and the other two phases are identified, i.e., there are sharp changes in χ_F at these phase boundaries, while in Fig. 5(b), only H_λ affects χ_F and the boundaries between insulating phase II and the other two phases are identified. The combination of the two contour maps in Figs. 5(a) and 5(b) is consistent with the phase diagram shown in Fig. 1. In Fig. 5(c), both H_λ's and H_μ's effects on χ_F and the corresponding contour map itself can reflect the phase diagram. In Figs. 5(a)–5(c), the χ_F variation in insulating phase II is not smooth, which is due to the possibility that the gap between E_0 and E_γ may be close to zero at some parameters [see Eq. (9)]. For this, the logarithmic plots of the gap ΔE for the first excited-state eigenenergy E_1 and ground-state eigenenergy E_0 varying with (λ,μ) are shown in Fig. 6. One sees that in phase II, all the values of ΔE are very small and some almost are equal to zero; therefore the fidelity F changes sharply at these parameter points. It is interesting that the contour map of ΔE divides the parameter space into three regions, which is also consistent with the phase diagram shown in Fig. 1.

In order to study the critical behavior around critical points (λ_c,μ_c), we study the finite scaling analysis of FS (Refs. 13 and 15–17) and obtain the corresponding critical exponents. It has been found that these critical exponents and the different scaling behaviors of FS can characterize the universality classes of phase transitions.[15] First, we study the transition between metallic phase I and metallic phase III and choose the critical point $(\lambda_c=1.0,\mu_c=1.0)$ as an example.

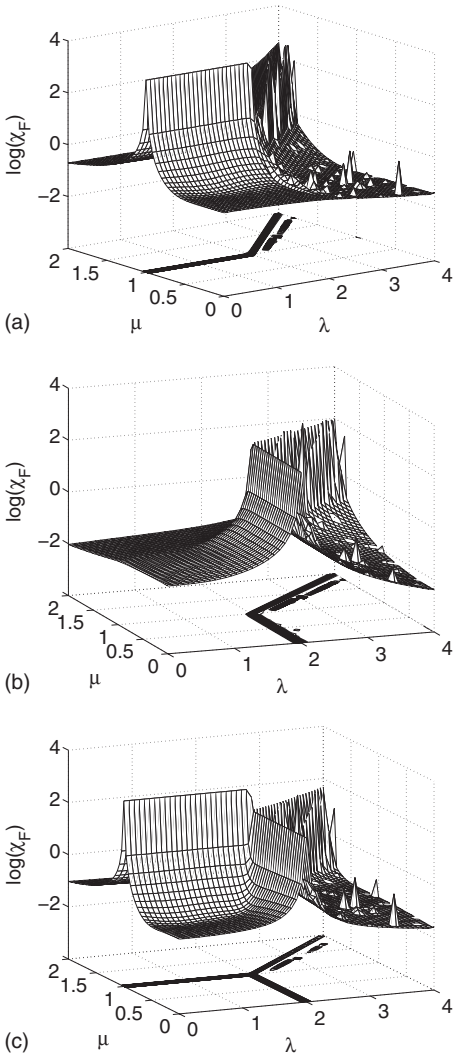

FIG. 5. The logarithmic plots of fidelity susceptibility χ_F and its contour maps as functions of (λ,μ) from different parameter paths $q=q(\lambda,\mu)$. The tangent unit vector (n^λ,n^μ) of paths is equal to (a) (0,1), (b) (1,0), and (c) $(1/\sqrt{5},-2/\sqrt{5})$.

Near the critical parameter with the tangent unit vector $(n^\lambda=0,n^\mu=1)$ of parameter paths, the χ_F is calculated for various system sizes N, which corresponds to the case that shown in Fig. 6(a). Along the parameter path, the FS reaches its maximum value $\chi_{F\max}$ at a certain position $\mu_{\max}$. The

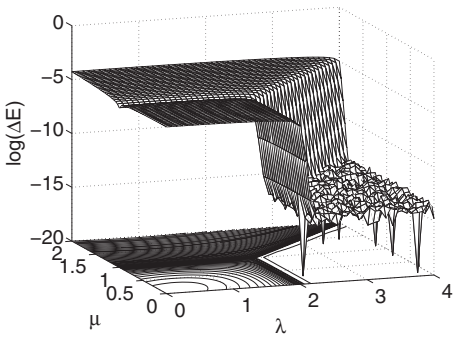

FIG. 6. $\log(\Delta E)$ varying with (λ,μ). Here ΔE is the gap between E_1 and E_0 at (λ,μ).

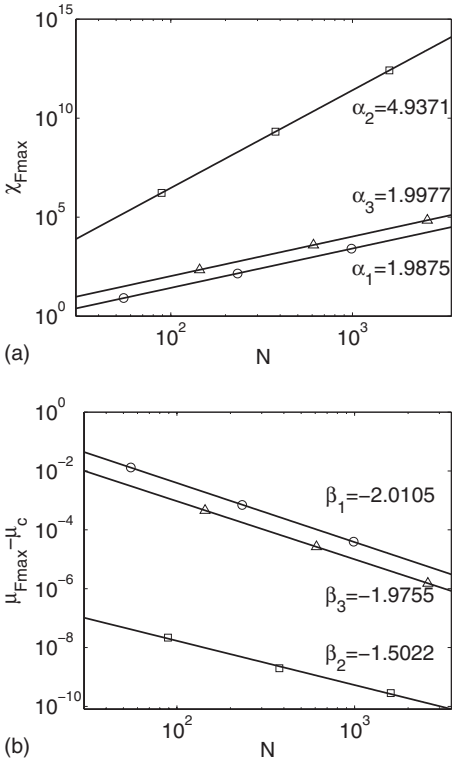

FIG. 7. The scaling behaviors of (a) $\chi_{F\max}$ and (b) $\mu_{F\max}-\mu_c$. The system sizes $F_{3l}=55, 233, 987$ (○), $F_{3l+1}=89, 377, 1597$ (□), and $F_{3l+2}=144, 610, 2584$ (△). At the same time, the corresponding fitted lines are also shown.

scaling behaviors of $\chi_{F\max}$ and $\mu_{F\max}-\mu_c$ are given in Figs. 7(a) and 7(b), respectively, which show that $\chi_{F\max}\propto N^\alpha$ and $\mu_{F\max}-\mu_c\propto N^\beta$. All $\beta<0$, which means that $\mu_{F\max}$ tends to the critical point μ_c in the thermodynamic limit. For the system sizes, N are chosen to be the Fibonacci number F_m with $m=3l+1$ and $m\neq 3l+1$ for integer l; the system sizes are divided into two cases.[36] It is found that $\alpha\approx 2.0$ and $\beta\approx -2.0$ for $m\neq 3l+1$, while $\alpha=4.9371$ and $\beta=-1.5022$ for $m=3l+1$. In Fig. 8, the corresponding scaling functions are plotted. It shows that the exponent $\nu\approx 1.0$ for $m\neq 3l+1$, while $\nu=2.4718$ for $m=3l+1$. Although the values of $\alpha(\beta)$ are different for $m=3l+1$ and $m\neq 3l+1$, the scaling relation $\alpha/\nu\approx 2$ is universal. The scaling relation is the same as that for a one-dimensional asymmetric Hubbard model studied by Gu *et al.*[15]

To understand the different behaviors between the systems with $N=F_{3l+1}$ and $N\neq F_{3l+1}$, we carefully analyze the structure of the system. According to the Fibonacci numbers $F_m=F_{m-2}+F_{m-1}$ with $F_0=F_1=1$, F_{3l} and F_{3l+1} are odd, which can be written as $2k_1+1$ and $2k_2+1$ with integers k_1 and k_2, respectively. For $N=F_{3l+1}$, $\phi=\frac{F_{3l}}{F_{3l+1}}=\frac{2k_1+1}{2k_2+1}$, and $\mu=1$, the hopping term in Eq. (3), $-[1+\mu e^{2\pi i\phi(n+1/2)}]=-[1+e^{2\pi i[(2k_1+1)/(2k_2+1)][(2n+1)/2]}]=0$ at the site $n=k_2$; i.e., a bond between the k_2th and (k_2+1)th sites breaks. The system is divided into two segments. For $N\neq F_{3l+1}$, it does not happen. This induces differences between the energy spectrum for systems with $N=F_{3l+1}$ and $N\neq F_{3l+1}$.[36]

Second, we study the transition between metallic phase I and insulating phase II and choose the critical parameter

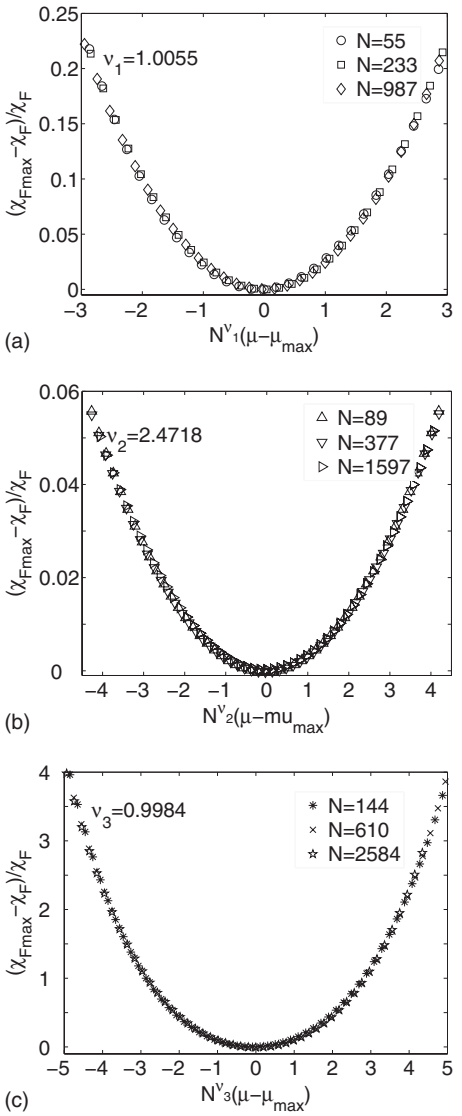

FIG. 8. The finite-size scaling analysis is performed for $(\chi_{F\max}-\chi_F)/\chi_F$ as a function of $N^{\nu}(\mu-\mu_{\max})$.

$(\lambda_c=2.0,\ \mu_c=0.5)$ as an example. Near the critical parameter with the tangent unit vector $(n^{\lambda}=1,\ n^{\mu}=0)$, the FS χ_F is calculated for various system sizes N, which corresponds to the case shown in Fig. 6(b). From Figs. 9 and 10, it is found that for all system sizes $55,89,\ldots,2584$, the values of α (β and ν) are the same and the scaling relation $\alpha/\nu\approx 2$ is also obtained. We have studied the transition between metallic phase III and insulating phase II; the results are similar and the relation $\alpha/\nu\approx 2$ is also tenable.

C. von Neumann entropy

The von Neumann entropy has been found to be a suitable quantity for characterizing the localization properties of electronic states.[25,28,29] Figures 11(a) and 11(b) show the site-averaged von Neumann entropy E_v^{γ} for the lowest edge states and the spectrum-averaged von Neumann entropy $\langle E_v\rangle$, respectively. The variations of the two quantities with respect to the parameter (λ,μ) are similar. $E_v^{\gamma}(\langle E_v\rangle)$ is near one in metallic phases I and III and relatively small in insulating phase II. There are sharp decreases in $E_v^{\gamma}(\langle E_v\rangle)$ at phase boundaries. Their contour maps divide the parameter space into three parts, which is consistent with the phase diagram shown in Fig. 1.

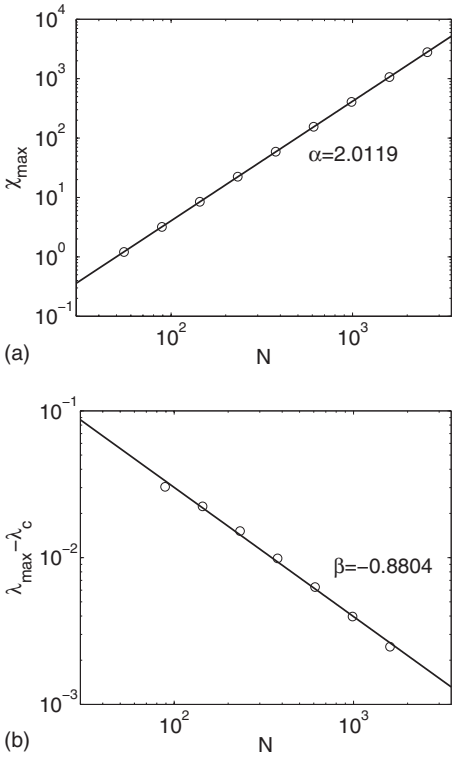

FIG. 9. The scaling behaviors of (a) $\chi_{F\max}$ and (b) $\lambda_{F\max}-\lambda_c$. The system sizes are $55,89,\ldots,2584$.

Conventionally, the inverse participation ratio (IPR) is often used as a measure of the wave-function localization length.[39] The larger the IPR is, the more delocalized the eigenstate is. It has been found that the site-averaged von Neumann entropy E_v^{γ} increases exponentially with the IPR (Ref. 29); i.e., E_v^{γ} can reflect the localization properties of electronic states. Figures 12(a)–12(d) show E_v^{γ} varying with eigenenergy E_{γ} for $(\lambda,\mu)=(1.0,0.5)$, (3.0,0.75), (1.0,1.0), and (2.0,0.5), which correspond to the metallic phase, the insulating phase, the MMT and the MIT, respectively. In Fig.

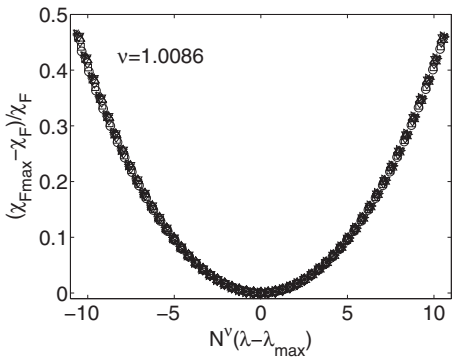

FIG. 10. The finite-size scaling analysis is performed for $(\chi_{F\max}-\chi_F)/\chi_F$ as a function of $N^{\nu}(\lambda-\lambda_{\max})$ for the system sizes are $55,89,\ldots,2584$.

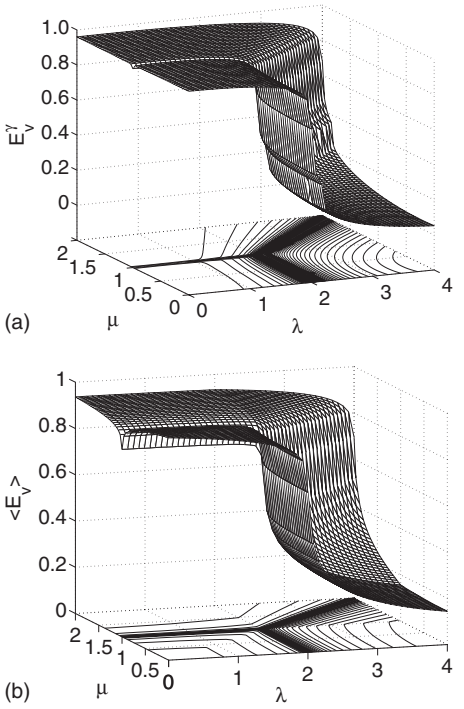

FIG. 11. The site-averaged von Neumann entropy E_v^γ for the lowest edge states (a) and the spectrum-averaged von Neumann entropy $\langle E_v \rangle$ (b) as functions of (λ, μ).

12(a), almost all the E_v^γ are near one, which means these states are delocalized. Comparing Fig. 12(b) with Fig. 12(a), all the E_v^γ are small, which means that all eigenstates are localized. In Figs. 12(c) and 12(d), there coexist large, intermediate, and small E_v^γ, which means the eigenstates are critical. Though all eigenstates for the three phase boundaries and the bicritical point are critical, the values of the spectrum-averaged von Neumann entropy $\langle E_v \rangle$ are different. Comparing these, the $\langle E_v \rangle$ for boundaries between metallic phases I and III are large, those for the bicritical point are intermediate, and those for boundaries between the metallic and insulating phases are small [see Fig. 11(b)]. All these indicate that, judging from the variation of the von Neumann entropy with parameter (λ, μ), the phase diagram can be completely characterized.

IV. CONCLUSIONS AND DISCUSSIONS

For the extended Harper model introduced in Ref. 36, we have studied the fidelity between the two lowest band-edge states corresponding to different model parameters, the FS and the von Neumann entropy of the lowest band-edge states, and the spectrum-averaged von Neumann entropy. All the three quantities can well characterize the rich phase diagram of the interesting model.

In detail, first, the variation of fidelity with parameters (λ, μ) for seven groups of fixed values of (λ_0, μ_0) is studied, which correspond to different phases, different phase boundaries, and the bicritical point. When parameters are in the same phase or same boundary, the fidelity is near one; otherwise, it is small. There are drastic changes in fidelity when one parameter is at phase boundary. At the same time, the contour maps of fidelity divide the parameter space into three regions, in agreement with the phase diagram of the model. In fact, these conclusions are valid for arbitrary fixed values

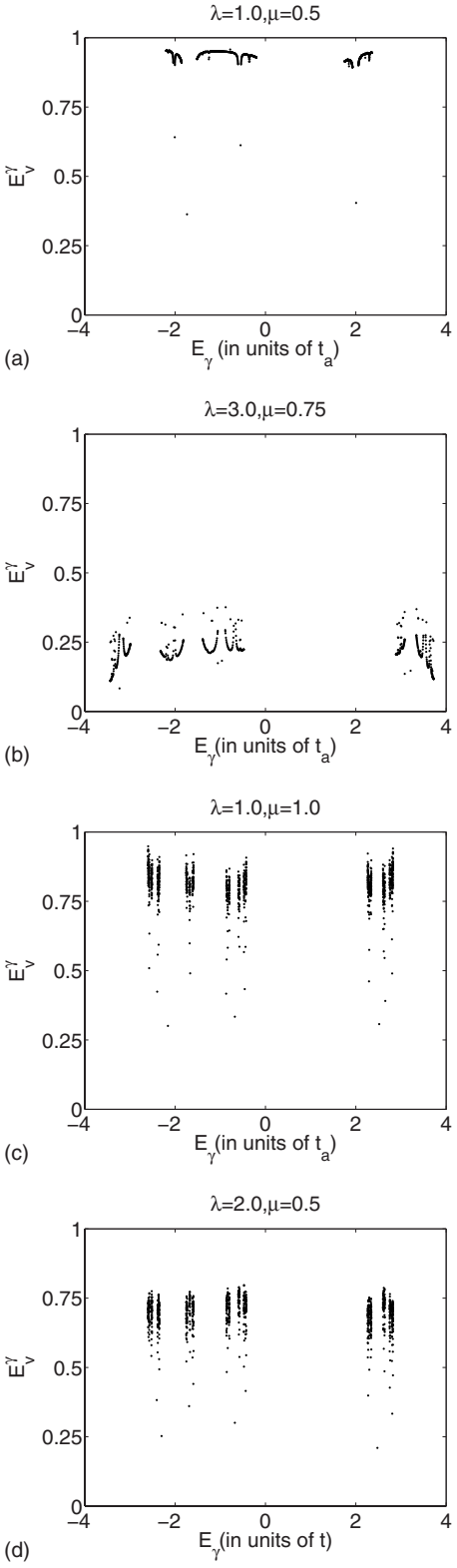

FIG. 12. The site-averaged von Neumann entropy E_v^γ varying with eigenenergy E_γ at $(\lambda, \mu)=(1.0, 0.5)$, (3.0,0.75), (1.0,1.0), and (2.0,1.0) for (a), (b), (c), and (d), respectively.

(λ_0, μ_0) in the parameter space. It indicates that the fidelity can well reflect the different phases and reveal different phase transitions.

Second, the FS is studied and the finite scaling analysis is performed for the MMT and the MIT. The contour maps of FS can well reflect the phase diagram. At the MMT, the critical exponents $\alpha(\beta, \nu)$ for system sizes $F_{m=3l+1}$ and $F_{m\neq 3l+1}$ are different, but the relation $\nu/\alpha \approx 2$ is universal. At the MIT, the critical exponents for all system sizes are the same and the relation $\nu/\alpha \approx 2$ is also tenable. Additionally, we have calculated the fidelity and FS based on other eigenstates and found that their variations with parameters are similar as that for the lowest band-edge states.

At last, the von Neumann entropy is studied. It is near one in the metallic phase, while it is small in the insulating phase. There are sharp changes at phase boundaries. There are differences in the values of spectrum-averaged von Neumann entropy for the three phase boundaries and the bicritical point. The contour maps of the von Neumann entropy are consistent with the phase diagram. All these indicate that the different phases and phase transitions can be completely distinguished by the von Neumann entropy.

ACKNOWLEDGMENTS

We would like to thank Zhongxia Yang for a critical reading of the paper and useful discussions. This project was supported by the National Natural Science Foundation of China (Grants No. 90203009 and No. 10674072), by the Specialized Research Fund for the Doctoral Program of Higher Education (Grant No. 20060319007), and by National Key Projects for Basic Research of China (Grant No. 2009CB929501). L.G. is supported in part by the Nature Science Foundation of Jiangsu Province of China (Grant No. 08KJB140005).

*lygong@njupt.edu.cn

†Corresponding author; pqtong@njnu.edu.cn

[1] M. A. Nielsen and I. L. Chuang, *Quantum Computation and Quantum Information* (Cambridge University Press, Cambridge, England, 2000).

[2] See, for example, *The Physics of Quantum Information*, edited by D. Bouwmeester, A. Ekert, and A. Zeilinger (Springer, Berlin, 2000).

[3] P. Zanardi and N. Paunkovic, Phys. Rev. E **74**, 031123 (2006).

[4] T. J. Osborne and M. A. Nielsen, Phys. Rev. A **66**, 032110 (2002).

[5] A. Osterloh, L. Amico, G. Falci, and R. Fazio, Nature (London) **416**, 608 (2002).

[6] S. Sachdev, *Quantum Phase Transitions* (Cambridge University Press, Cambridge, England, 1999).

[7] M. Cozzini, P. Giorda, and P. Zanardi, Phys. Rev. B **75**, 014439 (2007).

[8] N. Paunković and V. R. Vieira, Phys. Rev. E **77**, 011129 (2008).

[9] P. Buonsante and A. Vezzani, Phys. Rev. Lett. **98**, 110601 (2007).

[10] N. Oelkers and J. Links, Phys. Rev. B **75**, 115119 (2007).

[11] S. Chen, L. Wang, S. J. Gu, and Y. Wang, Phys. Rev. E **76**, 061108 (2007).

[12] P. Zanardi, H. T. Quan, X. G. Wang, and C. P. Sun, Phys. Rev. A **75**, 032109 (2007).

[13] W. L. You, Y. W. Li, and S. J. Gu, Phys. Rev. E **76**, 022101 (2007).

[14] L. Campos Venuti, M. Cozzini, P. Buonsante, F. Massel, N. Bray-Ali, and P. Zanardi, Phys. Rev. B **78**, 115410 (2008).

[15] S. J. Gu, Ho Man Kwok, W. Q. Ning, and H. Q. Lin, Phys. Rev. B **77**, 245109 (2008).

[16] H. M. Kwok, W. Q. Ning, S. J. Gu, and H. Q. Lin, arXiv:0710.2581, Phys. Rev. E (to be published).

[17] S. Yang, S. J. Gu, C. P. Sun, and H. Q. Lin, Phys. Rev. A **78**, 012304 (2008).

[18] M.-F. Yang, Phys. Rev. B **76**, 180403(R) (2007).

[19] Y.-C. Tzeng and M. F. Yang, Phys. Rev. A **77**, 012311 (2008).

[20] S. Chen, L. Wang, Y. J. Hao, and Y. P. Wang, Phys. Rev. A **77**, 032111 (2008).

[21] H. Q. Zhou, J. H. Zhao, and B. Li, arXiv:0704.2940 (unpublished).

[22] H. Q. Zhou, J. H. Zhao, H. L. Wang, and B. Li, arXiv:0711.4651 (unpublished).

[23] P. Zanardi, Phys. Rev. A **65**, 042101 (2002).

[24] S. J. Gu, S. S. Deng, Y. Q. Li, and H. Q. Lin, Phys. Rev. Lett. **93**, 086402 (2004).

[25] L. Y. Gong and P. Q. Tong, Phys. Rev. E **74**, 056103 (2006).

[26] F. Buscemi, P. Bordone, and A. Bertoni, Phys. Rev. A **73**, 052312 (2006).

[27] D. Larsson and H. Johannesson, Phys. Rev. A **73**, 042320 (2006).

[28] L. Y. Gong and P. Q. Tong, Phys. Rev. A **71**, 042333 (2005).

[29] L. Y. Gong and P. Q. Tong, Phys. Rev. B **76**, 085121 (2007).

[30] D. R. Hofstadter, Phys. Rev. B **14**, 2239 (1976).

[31] F. H. Claro and G. H. Wannier, Phys. Rev. B **19**, 6068 (1979).

[32] S. Aubry and G. Andre, Ann. Isr. Phys. Soc. **3**, 133 (1980).

[33] J. B. Sokoloff, Phys. Rep. **126**, 189 (1985).

[34] J. H. Han, D. J. Thouless, H. Hiramoto, and M. Kohmoto, Phys. Rev. B **50**, 11365 (1994).

[35] Y. Takada, K. Ino, and M. Yamanaka, Phys. Rev. E **70**, 066203 (2004).

[36] K. Ino and M. Kohmoto, Phys. Rev. B **73**, 205111 (2006).

[37] P. Zanardi, P. Giorda, and M. Cozzini, Phys. Rev. Lett. **99**, 100603 (2007).

[38] C. H. Bennett, H. J. Bernstein, S. Popescu, and B. Schumacher, Phys. Rev. A **53**, 2046 (1996).

[39] B. Kramer and A. MacKinnon, Rep. Prog. Phys. **56**, 1469 (1993).